Wave Motion 94 (2020) 102515

Contents lists available at ScienceDirect

Wave Motion

journal homepage: www.elsevier.com/locate/wamot

Synthesis of highly convergent 2D and 3D finite elements for short acoustic wave simulation

Dalia Čalnerytė *, Andrius Kriščiūnas, Rimantas Barauskas

Department of Applied Informatics, Faculty of Informatics, Kaunas University of Technology, Studentu St. 50-407, LT-51368, Kaunas, Lithuania

ARTICLE INFO

Article history:
Received 21 May 2019
Received in revised form 14 January 2020
Accepted 15 January 2020
Available online 18 January 2020

Keywords:
Finite element model
Modal synthesis
Short wave propagation

ABSTRACT

New higher-order finite elements of enhanced convergence properties for acoustic wave simulation are presented in the paper. The element matrices are obtained by combining modal synthesis and optimization techniques in order to achieve minimum errors of higher modes of the computational domain. As a result, simulation models of propagating wave pulses require a smaller number of finite element divisions per wavelength compared to the conventional element model thus significantly reducing computational costs. Though finite element matrices are obtained in optimization, the resulting patterns of the matrices are versatile and further can be used in any wave propagation model. The mass matrices of the elements are diagonal, so explicit time integration schemes are applicable. The usage of new elements is especially efficient in situations where wavelengths of the simulated signal are much shorter than the dimensions of the computational domain. This is referred to as short wave propagation analysis. The results of wave propagation simulation for ultrasonic measurements are presented as application examples. The B-scans and computed dispersion curves are provided for visual interpretation of the results.

1. Introduction

One of the "weak spots" of the finite element (FE) models is the analysis of wave propagation in the domains, the dimensions of which many times exceed the characteristic wavelength. In this paper we refer to such situations as short acoustic or elastic wave simulation. As in the other research [1,2], the term "short wave" is not related to a certain range of frequencies or wavelengths [3]. It is used to represent the ratio of the dimensions of the computational domain against the characteristic wavelength. In this sense, short wave analysis could be encountered during wave pulse simulation in the acoustic environment [4], simulation of the seismic signal [5,6], etc.

Severe wave shape distortions may take place after the wave pulse propagation is simulated over a distance which covers many wavelengths. The main reason is the erroneous representation of the higher modal frequencies of the domain. Due to these errors the harmonic components, which comprise the wave pulse, propagate with different velocities and finally the resulting wave shape may become very different from the one observed in reality. A well-known and universal solution for diminishing the model errors is a refinement of the finite element mesh. The number of elements per wavelength is individual for each case and should be determined after convergence analysis with respect to the dimensions of the model and the highest frequency in the pulse. In some cases 17–20 FE per wavelength is used to get sufficient

* Corresponding author.
E-mail addresses: dalia.calneryte@ktu.lt (D. Čalnerytė), andrius.krisciunas@ktu.lt (A. Kriščiūnas), rimantas.barauskas@ktu.lt (R. Barauskas).

https://doi.org/10.1016/j.wavemoti.2020.102515
0165-2125/

accuracy [7], in other situations even up to 35 FE per wavelength are necessary in order to obtain acceptable representation of the wave pulses propagating over considerable distances [8]. Since finer FE mesh requires smaller numerical time integration step, bigger rounding errors accumulate as the number of time steps increases. If a smaller number of FE per wavelength is used, the numerical errors occur. They visually resemble the wave reflections from the model nodes. The pulse shape gets more distorted the longer distance the pulse propagates. Thus, the simulation models of practical importance may contain millions of FE making such problems hardly possible to solve [2].

The investigation related to the short wave simulation problem in FE models has been the subject of research for decades. Satisfactory simulation results may be obtained with reasonable computational resources by adding appropriate boundary conditions [9], decomposing the computational domain [10] or applying computationally cheaper modifications of the finite element method (FEM) with preconditions such as constant shape of the cross-section [11,12]. Multiscale modeling was used to simulate wave propagation in a structure composed of materials with significantly different properties [13]. If geometrical and mechanical properties in waveguides are uniform in one direction, semi-analytical FEM can be applied for the simulation. In such cases harmonic space and time laws are assumed along the direction of wave propagation, whereas the cross-section of the waveguide is modeled by the finite elements in a lower space dimensionality [11].

However, the standard FEM remains one of the most widely used methods because of its versatility. Many researchers investigate the mathematical background of FEM in order to find the best solution for reducing numerical errors, which occur in simulations of wave propagation. It has been shown that the numerical dispersion can be reduced if the Gauss or Gauss–Labatt numerical integration points over the FE area are employed [14]. The application of Labatt or Chebyshev abscises in combination with the generalized mass matrices can be applied to obtain a reasonable solution [15]. The research on the lumped mass matrix redistribution for higher-order elements are presented in [16,17]. It has been demonstrated that the numerical dispersion can be reduced by applying the template proposed in [18] for 1D higher-order element under the combination of several minimization parameters such as the locations of the inner nodes of finite elements or the weight coefficients of shape functions. The better convergence for a 2D triangular FE model has been obtained by shifting integration points of the element shape function away from their conventional positions [19]. The numerical integration scheme with additional step to filter numerical errors is presented in [20].

Usually, the proposed scheme is compared to the theoretical solutions or the results obtained by the conventional computational schemes [21,22] based on one selected criterion of accuracy or computational efficiency. Employment of coarser FE meshes does not necessarily mean that the computational resources will be lower compared to the models assembled of the first-order FEs with lumped mass matrices. The computational costs may also depend on both the bandwidths of matrices and certain additional calculations, such as numerical noise filtering procedures involved in numerical integration. The use of higher-order mass matrices seriously reduces the efficiency of the explicit dynamic analysis schemes. Even in case of higher-order FE with diagonal mass matrices, the stiffness matrix bandwidth in the models is wider and simulations require more computational memory and higher number of arithmetical operations. Moreover, in case of unequal distribution of mass between the inner nodes of the higher-order element, the time step of numerical integration must be smaller in order to ensure accuracy and stability of the numerical integration scheme.

In this paper we expand the mode synthesis technique for FE construction, which has been originally presented in [8]. Despite the high convergence properties of the earlier models, the synthesized mass matrices were non-diagonal and not well-suited for explicit analysis. A modification of the algorithm has been proposed for 1D case in [23], where the synthesized elements with diagonal mass matrices have been obtained. The adaptation of the algorithm for the 2D case has been proposed in [24]. In this paper we finalize the acoustic case by introducing the computationally cheaper synthesis technique which enables the construction of finite elements in 2D and 3D.

2. Fundamentals

The constant density acoustic wave equation is considered in this paper [25]:

$$\ddot{u} = c^2 \nabla^2 u + f \tag{1}$$

where $u(t, x)$ is the pressure wavefield, $\ddot{u}$ represents its second-order temporal derivative, c is the wave velocity, ∇^2 is the Laplacian and f defines the source.

Despite the dimensions of the analysis (1D, 2D or 3D), the finite element model of short wave propagation in acoustic medium can be presented in the form of the general structural dynamic equation system:

$$[\mathrm{M}]\left\{\ddot{\mathrm{U}}\right\} + [\mathrm{C}]\left\{\dot{\mathrm{U}}\right\} + [\mathrm{K}]\{\mathrm{U}\} = \{\mathrm{F(t)}\} \tag{2}$$

where [M], [C] and [K] are mass, damping and stiffness matrices, {U} is the vector of nodal variables and {F(t)} is the excitation vector. In case of small damping, the damping matrix has a negligible impact on the eigen solution of the model, therefore [C] = 0 can be assumed. If damping cannot be neglected, the proportional damping model as $[\mathrm{C}] = a[\mathrm{M}] + \beta[\mathrm{K}]$ is used with appropriate coefficients a, β. Structural matrices are assembled of element matrices using the standard assembly procedure. The structural element matrices are obtained as follows:

$$\left[\mathrm{M}^e\right] = \rho \int_{Ve} \left[\mathrm{N}^e(\mathrm{x})\right]^{\mathrm{T}} \left[\mathrm{N}^e(\mathrm{x})\right] dV \tag{3.1}$$

$$\left[K^e\right] = \int_{Ve} [B]^T [D] [B] dV \tag{3.2}$$

where ρ is mass density of the medium, V_e is the element volume, $[N^e(x)]$ is a vector of linear element shape functions, [D] is an elasticity matrix, [B] is a gradient matrix. The matrix $[M^e]$ obtained in Eq. (3.1) is a consistent mass matrix. If this type of mass matrix is used in simulation, it slows down the calculations. Diagonalization of the mass matrix does not change modal frequencies significantly [23]. That is why the lumped mass matrix is used in the element synthesis and numerical examples.

There are two main approaches to model wave propagation in the acoustic medium [26–28]. If the acoustic problem is formulated using the simplification of solid mechanics, shear modulus is assumed to be 0. The obtained formulation is a vectorial field problem. Although it is possible to calculate pressure as a mean of axial stress components, this approach is not cost-effective. Using this approach, 2 degrees of freedom in 2D and 3 degrees of freedom in 3D must be calculated at each node to get one pressure variable which defines the problem. Another approach is a simplification of the dynamic problem in compressive fluids by constructing acoustic finite element. The field variables in the fluid dynamics are velocity and pressure. Although this classifies the problem as a vectorial field problem, it can be reformulated to the scalar field problem with pressure as a state variable. The simplification is an efficient approach, which requires modest computational resources.

The elasticity matrix of such elements is given by:

$$[D] = E[I] \tag{4}$$

where E is stiffness modulus of the medium, [I] is a 2×2 identity matrix for 2D and 3×3 identity matrix for 3D case. The corresponding gradient matrix is given by:

$$[B] = [\partial] [N^e(x)] \tag{5}$$

where $[\partial]$ is a 2×1 vector of gradient operators and $[N^e(x)]$ is a 1×4 vector of element shape functions for 2D case and 3×1 and 1×8 vectors for 3D cases respectively. The dimensions of the resulting gradient matrix [B] are 2×4 for 2D and 3×8 for 3D case.

The theoretical wave speed value in homogeneous isotropic medium is calculated analogously to the 1D elastic wave case:

$$v_{st} = \sqrt{E/\rho} \tag{6}$$

3. Synthesis of the element

In case of non-damped or proportionally damped structures, structural equation (2) can be presented in modal coordinates of the non-damped structure. Modal frequencies (MF) and modal shapes (MS) of the structure are obtained by solving the following eigenvalue problem corresponding to Eq. (2):

$$\left([K] - \omega^2 [M]\right) \{y\} = \{0\} \tag{7}$$

where ω is modal frequency, $\{y\}$ is modal shape. Real symmetric structural matrices [M] and [K] ensure the solutions of (7) as n structural modes ω_i, $\{y_i\}$, $i = 1, \ldots, n$, here n is the number of degrees of freedom. The fundamental properties of structural modes provide that matrices [K] and [M] can be expressed in terms of normalized mode shapes and mode frequencies as:

$$[K] = \left([Y]^T\right)^{-1} \left[\text{diag}\left(\omega_1{}^2, \omega_2{}^2, \ldots, \omega_n{}^2\right)\right] [Y]^{-1} \tag{8.1}$$

$$[M] = \left([Y]^T\right)^{-1} [Y]^{-1} \tag{8.2}$$

where $[Y] = [\{y_1\}, \{y_2\}, \ldots, \{y_n\}]$. Generally, the Eq. (2) is the same for one finite element and for the whole FE model, and can be expressed using element matrices in Eq. (8) [3,29]. It should be noted that the mass matrix (8.2) is not changed during the synthesis process as the lumped mass is used in the simulations.

The synthesis algorithm is based on the assumption that if the simulation of the pulse propagation works well in a sample structure assembled of large number of the independent elements, such independent elements can be used in any structure assembled of such elements. That is why the objective of optimization is to minimize the numerical errors generated for the sample structure assembled of the synthesized elements. The optimization variables are matrix $[a^y]$ and vector $\{a^\omega\}$ of correction coefficients which are applied to make corrections of element modes as:

$$\left[\text{diag}\left(\tilde{\omega}_1{}^2, \tilde{\omega}_2{}^2, \ldots, \tilde{\omega}_n{}^2\right)\right] = \left[\text{diag}\left(a_1^\omega \omega_1{}^2, a_2^\omega \omega_2{}^2, \ldots, a_n^\omega \omega_n{}^2\right)\right] \tag{9.1}$$

$$\left[\left\{\tilde{y}_1\right\}, \ldots, \left\{\tilde{y}_n\right\}\right] = \left[\{a_1^y\} \circ \{y_1\}, \ldots, \left\{a_n^y\right\} \circ \{y_n\}\right] \tag{9.2}$$

where $\left\{\tilde{y}_i\right\}$, $\tilde{\omega}_i$ are ith modal shape and modal frequency of the synthesized element, $\{a_i^y\} \circ \{y_i\}$ is the result of an element-wise multiplication of ith columns of matrices $[a^y]$ and $\{a^\omega\}$. At the initial step optimization variables are equal to 1 and correspond to the conventional element. The first mode represents rigid body and it is not modified in order to preserve

the fundamental properties of the element. Moreover, its frequencies are always equal to 0 and an error is not generated for this mode. The objective function presents the cumulative error of the first $2 \dots r$ eigenfrequencies of the sample domain with respect to the exact eigenfrequency values $\{\omega^*\}$ of the sample domain. The optimized range of frequencies is chosen with respect to the specific problem and number of nodes in the synthesized element. The higher percentage of frequencies can be optimized for the element with the higher number of nodes. This leads to the wider range of optimized frequencies if the larger sample structure is used in the optimization process. The minimization problem is formulated as follows:

$$\min_{[\mathrm{a}^y],\{\mathrm{a}^\omega\}} \Psi = \min_{[\mathrm{a}^y],\{\mathrm{a}^\omega\}} \sum_{i=2}^{r} \left(\frac{\hat{\omega}_i - \omega_i^*}{\omega_i^*} \right)^2 \tag{10}$$

where $\hat{\omega}_i$ is ith frequency of the sample domain assembled of the synthesized elements, ω_i^* is the exact value of the ith eigenfrequency of the sample domain. The exact values of eigenfrequencies are available only in 1D case. In 2D and 3D, the values of close-to-exact modal frequencies are used in Eq. (10). They are obtained for the structure of the same geometry as the sample domain by a mesh much denser than the mesh of the elements to be synthesized. First $1 \dots r$ modal frequency values of this structure are considered as close-to-exact and used in the objective function. To calculate close-to-exact modal frequencies, a mesh which is used in calculations should be fine enough to ensure that the frequency values converge to the exact solution in the optimized range. If the number of the optimized values increases, a finer mesh is required to satisfy this requirement. However, the computational resources often limit the density of the mesh.

It was demonstrated in [23] that it is possible to synthesize 10-node elements with the diagonal mass matrix in the 1D case that the structure assembled of such elements has almost 5 times coarser mesh and obtains the same numerical dispersion level as the structure assembled of the conventional elements. Unfortunately, the application of the same technique to 3D case is too expensive in the computational manner, as 10-node 1D elements contain 99 optimization variables (10×9 matrix $[\mathrm{a}^y]$ and 9-element vector $\{\mathrm{a}^\omega\}$), in 3D case the number of optimization variables for $10 \times 10 \times 10$ node element increase to 998 999 correction parameters (1000×999 matrix $[\mathrm{a}^y]$ and 999-element vector $\{\mathrm{a}^\omega\}$). Moreover, the eigenvalue problem must be solved for the sample structure at each optimization step and its complexity is $O(n^3)$, where n is number of nodes in the element. In order to overcome this problem, the approach of modal errors minimization over several simpler sample structures has been developed. In 2D and 3D cases the synthesis is based on the assumption that if the synthesized element works well in several significantly different sample structures, it also works well in any structure built of such elements. The sample structures used for the synthesis in 2D and 3D cases are presented in Fig. 1. The bigger sample generalizes the behavior of the synthesized element and signal transitions between the elements better as more connections (shared nodes) between the adjacent elements are included. However, the sample structure should be as small as possible because the eigenvalue computation of the complexity $O(n^3)$, where n is number of nodes in the structure, must be solved in each optimization step. The element syntheses in 2D and 3D cases are based on two and three sample domains correspondingly. Due to fact that the acoustic fields have no shear waves, more complex shapes of the sample domains are not necessary.

Finally, the optimization problem of the objective function with S sample structures reads as:

$$\min_{[\mathrm{a}^y],\{\mathrm{a}^\omega\}} \Psi = \min_{[\mathrm{a}^y],\{\mathrm{a}^\omega\}} \sum_{k=1}^{S} \sum_{i=2}^{r_s} \left(\frac{\hat{\omega}_{k,i} - \omega_{k,i}^*}{\omega_{k,i}^*} \right)^2 \tag{11}$$

where S is the number of sample structures, r_s is the number of the modal frequencies for which the modal errors are minimized, $\hat{\omega}_{k,i}$ is ith modal frequency of the kth sample structure assembled of the synthesized elements, $\omega_{k,i}^*$ is ith close-to-exact modal frequency of the kth sample structure.

The gradient descent method was employed for minimization. The gradient values have been obtained by the variational calculus relations in [8]. There is no general complexity estimation for the gradient descent method as the number of iterations depends on the prescribed tolerance. It is important to notice that the stiffness matrix of the synthesized element obtained in the synthesis process can be used as a template to construct FE of the same shape for any acoustic medium. To do this, it is enough to multiply the template of the stiffness matrix obtained by the described synthesis process by the stiffness modulus, because the elasticity matrix can be written as product of a constant (stiffness modulus) and an identity matrix (Eq. (3.2)). Such elements can be used in regular mesh domains without changing mass matrix of the element and keeping it in the diagonalized form of (3.1) [24]. Scaling of the elements is applied to construct a mesh of an appropriate density. The conventional element models converge independently on mass matrix type (consistent or lumped) used in simulations. The smaller numerical errors of the synthesized element in the pulse frequency range guarantee that the synthesized element does not work worse than the conventional element therefore the convergence of the synthesized element model is ensured. The flowchart for the synthesis process is provided in the Appendix (see Fig. A.1).

4. Numerical experiments

The first step of the numerical analysis is the construction of the synthesized element. After this step is performed, the constructed element can be used to simulate pulse propagation in various acoustic media. Although the element can be

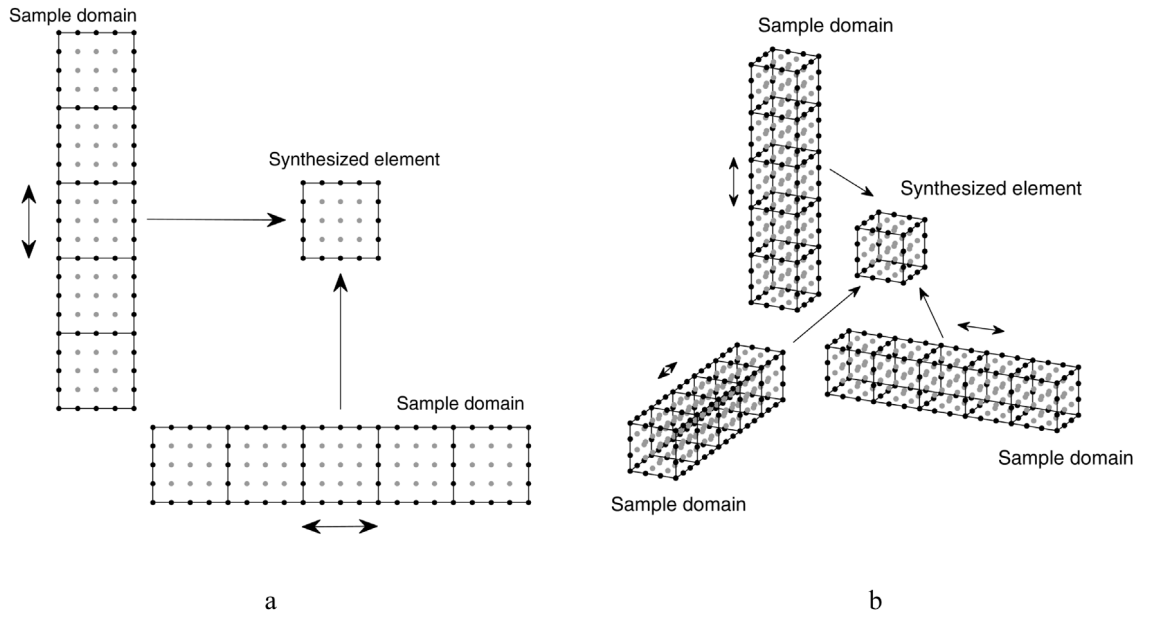

Fig. 1. Sample domains used for the synthesis process in 2D (a) and 3D (b).

synthesized to cover a specific range of frequencies, optimization of the prescribed number of first modes was performed in this research. The number of optimized frequencies was chosen empirically. The normalized modal frequency error e_i for ith mode is calculated as follows:

$$e_i = \frac{\hat{\omega}_i - \omega_i^*}{\omega_i^*} \tag{12}$$

where $\hat{\omega}_i$ is ith frequency of the sample domain assembled of the analyzed elements, ω_i^* is close-to-exact value of ith eigenfrequency of the sample domain. A computer with 64 GB RAM and Intel(R) Core (TM) i9-9900KF CPU 3.60 GHz was used in the syntheses and numerical experiments.

For the 2D case, the square synthesized element of 5 × 5 nodes (25 nodes in total) was used in the synthesis process. The distribution of the nodes in the element corresponds to the node distribution in the structure of 4 × 4 conventional linear elements. The rectangular sample domains (Fig. 1a) were constructed of 8 synthesized elements on the long side and 1 synthesized element on the short side. The close-to-exact frequencies of the sample domains were calculated for the conventional element structures using much finer mesh of the same geometry as the sample structures. The element side length of the fine mesh was 8 times smaller than the side length between the nodes of the synthesized element. The first 15 frequencies of the sample domain were taken into the objective function (11). On average, one iteration in the gradient descent optimization took approximately 0.85 s. The objective function obtained a value less than 10^{-5} in 2270 iterations. The errors obtained for the sample structures assembled of the synthesized elements and conventional elements with the same number of nodes are provided in Fig. 2a. Although only the first 15 frequencies are included in the optimization, the structure assembled of the synthesized elements generate significantly smaller errors compared to the conventional model in an almost twice wider range than optimized. Fig. 2b shows the comparison of the normalized modal frequency errors for the square structure of 8 × 8 synthesized elements (32 × 32 conventional elements for the same area domain). This demonstrates that the normalized frequency errors of the synthesized element model are smaller for the structure which was not used in the optimization.

The shorter sample domains and lower number of nodes in one axis were used to synthesize the element in 3D because the synthesis process in the 3D case requires significantly higher computational resources. The element of 4 × 4 × 4 nodes (64 nodes in total) was analyzed. Three rectangular parallelepiped sample domains (Fig. 1b) were constructed of 6 synthesized elements along one side and 1 synthesized element along the other two sides. The close-to-exact frequencies for the structures were computed for the mesh of rectangular parallelepiped with the side length six times smaller than the initial distance between the two nodes in the synthesized element. The lowest 5 frequencies were used in the optimization process. The average iteration time was 5.4 s in parallel computing mode. The objective function value reached values less than 10^{-5} after 1000 iterations. The normalized modal frequency errors for the 3D element are provided in Fig. 3. Although the errors for the first 5 modes of the synthesized element model are negligible, the improvement obtained for the synthesized element model is not significant for the higher frequencies. Due to the limitation of computational resources it was not possible to compare the frequencies of the more complex models. For example, to calculate the

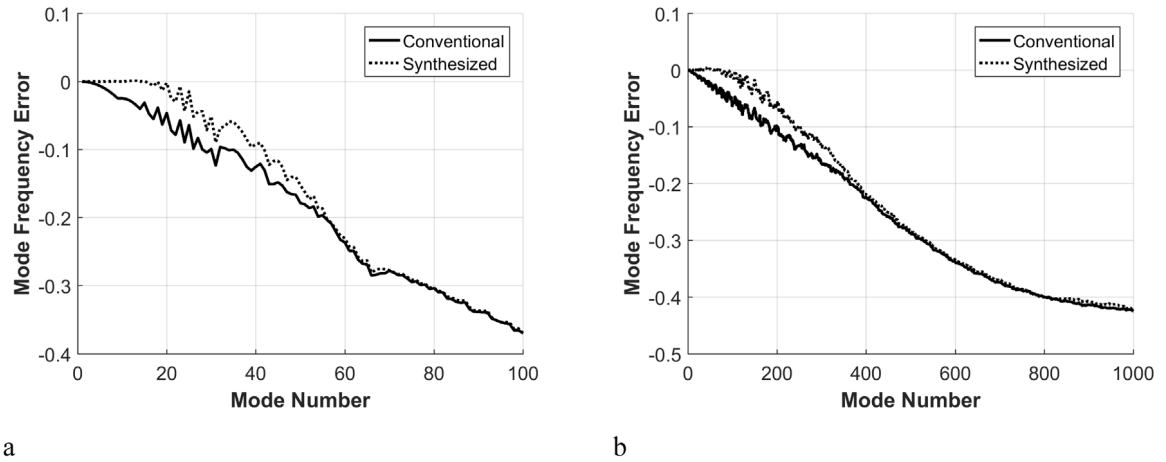

Fig. 2. The modal frequency error comparison of conventional and synthesized 2D elements (5 × 5 nodes) for a sample domain (a) of 8 × 1 synthesized elements (165 nodes) used in synthesis process and square domain (b) of 8 × 8 synthesized elements (1089 nodes).

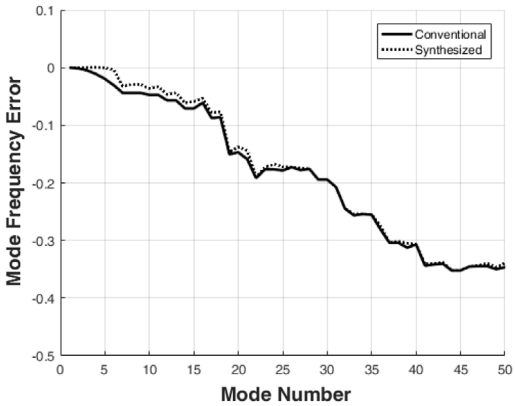

Fig. 3. The mode frequency error comparison of conventional and synthesized 3D elements (4 × 4 × 4 nodes) for a sample domain used in synthesis process (6 × 1 × 1 synthesized elements, 304 nodes).

close-to-exact modal values of the cube respective to 6 × 6 × 6 synthesized elements using the same density as in the previous structures (6 times shorter side length than the initial distance), the eigenvalue problem for 1 295 029 nodes should be solved. For the structures with approximately ten times smaller number of nodes respective to 6 × 3 × 1 synthesized elements (113 905 nodes), the construction of structural matrices and solving the eigenvalue problem takes over 1200 s. As the complexity of the eigenvalue problem is $O(n^3)$, it is not possible to solve the eigenvalue problem for the cube in a reasonable amount of time nor using available computational memory.

The second step of the numerical experiment was the simulation of the wave propagation in the structure of the arbitrary geometry. The results of wave propagation simulation in 2d and 3D cases are presented in Sections 4.1 and 4.2 respectively. The synthesized elements are squares in 2D case and rectangular parallelepiped in 3D case. The central difference time integration scheme was employed in the numerical experiments. The wave pulse shape was used for the propagating wave excitation in both 2D and 3D cases. The pulse is mathematically expressed as a sine wave multiplied by the Gaussian window:

$$u(t) = \exp\left(-a \cdot \left(\frac{t}{\mathrm{T}} - b\right)^2\right) \cdot \sin\left(\frac{2\pi f t}{\mathrm{T}}\right) \tag{13}$$

where $a = k_a f \sqrt{-\frac{2\ln 0.1}{p_s}}$; $b = \frac{2p_s}{3f}$, p_s is the number of periods, k_a is the asymmetry factor, f is the frequency and T denotes the period of the pulse and is applied to scale the impulse in time [30]. In the simulations we used the values as $p_s = 1.5$, $k_a = 5, f = 2$. The pulse period $T = 1$ was used as a reference unit in the numerical simulations. As the material properties are linear, the results are presented in the dimensionless form, which enables to scale the matrices and apply them for any specific medium. The values of stiffness modulus E and mass density ρ were equal to 1 in the numerical experiments.

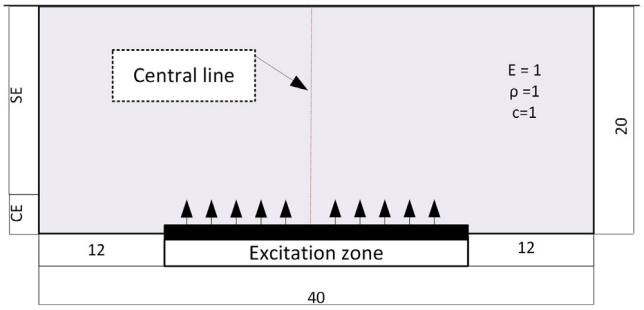

Fig. 4. The scheme of the geometry used in the 2D case.

The obtained results are compared with the results obtained for the conventional element model which contains the same number of nodes or is composed of finer meshes. Unfortunately, due to the limitations of computational resources, the comparison with fine mesh models was possible only for small structures.

4.1. Simulation of 2D acoustic wave

Propagation of the 2D acoustic wave given by Eq. (13) was simulated in a rectangular structure. The pulse length is equal to 1 because the wave speed in the dimensionless form is equal to 1. The length and the width of the structure were 40 and 20 pulse lengths respectively. These parameters correspond to 80 and 40 wavelengths. The excitation pulse was assigned for the nodes with Y coordinate equal to 0 and X coordinate in range from 12 to 28. The side length of the synthesized square element was equal to 0.16 resulting in the 0.04 distance between the two nodes and approximately 13 nodes per wavelength. The first row of synthesized elements (SE) was replaced with the same size area constructed of the conventional elements (CE) in the synthesized element model in order to assign exactly the same boundary conditions for both models. The scheme of the geometry used in the numerical experiments is shown in Fig. 4.

Values of the nodal variables along the central line nodes after simulation for 8 and 16 pulse periods T are provided in Fig. 5 for the coarse conventional element model, synthesized element model and fine conventional element model with element side length twice smaller than in the coarse model. It can be noticed that at 8 pulse periods the pulse shape in the model of coarse conventional elements deteriorated significantly. However, even after 16 pulse periods the pulse shape in the synthesized element model changed only slightly. The differences in the phase originate because of the modes which generate errors of different size in the conventional and synthesized element models. The difference becomes more noticeable as the pulse propagates.

The distribution of the state variable after the simulation for 20 pulse periods T is provided in Fig. 6 for conventional (Fig. 6a) and synthesized element (Fig. 6b) models. The B-scan views for the central line (X coordinate equal to 20) are provided for both models respectively in (Fig. 6c, d). B-scan view displays the propagation of the normalized values of the state variable along the chosen line during the analyzed period. In the error-free case the B-scan view is a straight line because all the harmonic components should propagate with the same velocity. The dispersion curve images display dispersion energy in a frequency–velocity domain [31]. The dispersion curves at the central line for both models are given in Fig. 6e, f. The theoretical dimensionless wave velocity is equal to 1 and is marked by the red dashed line. In simulations the line deflects from the straight direction, see black dotted lines in Fig. 6e, f. This means that the higher harmonic components propagate slower than the lower ones. Consequently, the shape of the simulated wave pulse changes as the wave propagates. This is referred to as the numerical dispersion of the propagating wave pulse. The smaller the difference between the theoretical curve and the curve obtained numerically, the smaller the numerical errors are generated in this frequency range. The results for the conventional elements structure are presented in Fig. 6e. In case the synthesized elements are used, the numerically obtained speed line remains close to theoretical over much wider frequency range, Fig. 6f. Consequently, the shape of the wave pulse remains correct during much longer propagation distance. If the synthesized elements are used in the model, the range of the close-to-exact frequencies is expanded approximately by 2.33 times as the curve obtained numerically drops to wave speed of 0.99 at 2.27 for the conventional element model and at 5.28 for the synthesized element model.

4.2. Simulation of 3D acoustic wave

Propagation of the 3D acoustic wave in a rectangular parallelepiped structure was analyzed. So that it would be possible to compare the results with the finer mesh model a simulation of pulse propagation in a short distance was performed. The signal of the form given by Eq. (13) was assigned to the nodes on one side of the structure. The length of the analyzed structure was 3.96 pulse lengths, the width and height were 0.84 pulse lengths. The side length of the synthesized element was equal to 0.12 resulting in an initial distance between the two nodes equal to 0.04 and approximately 13 nodes per

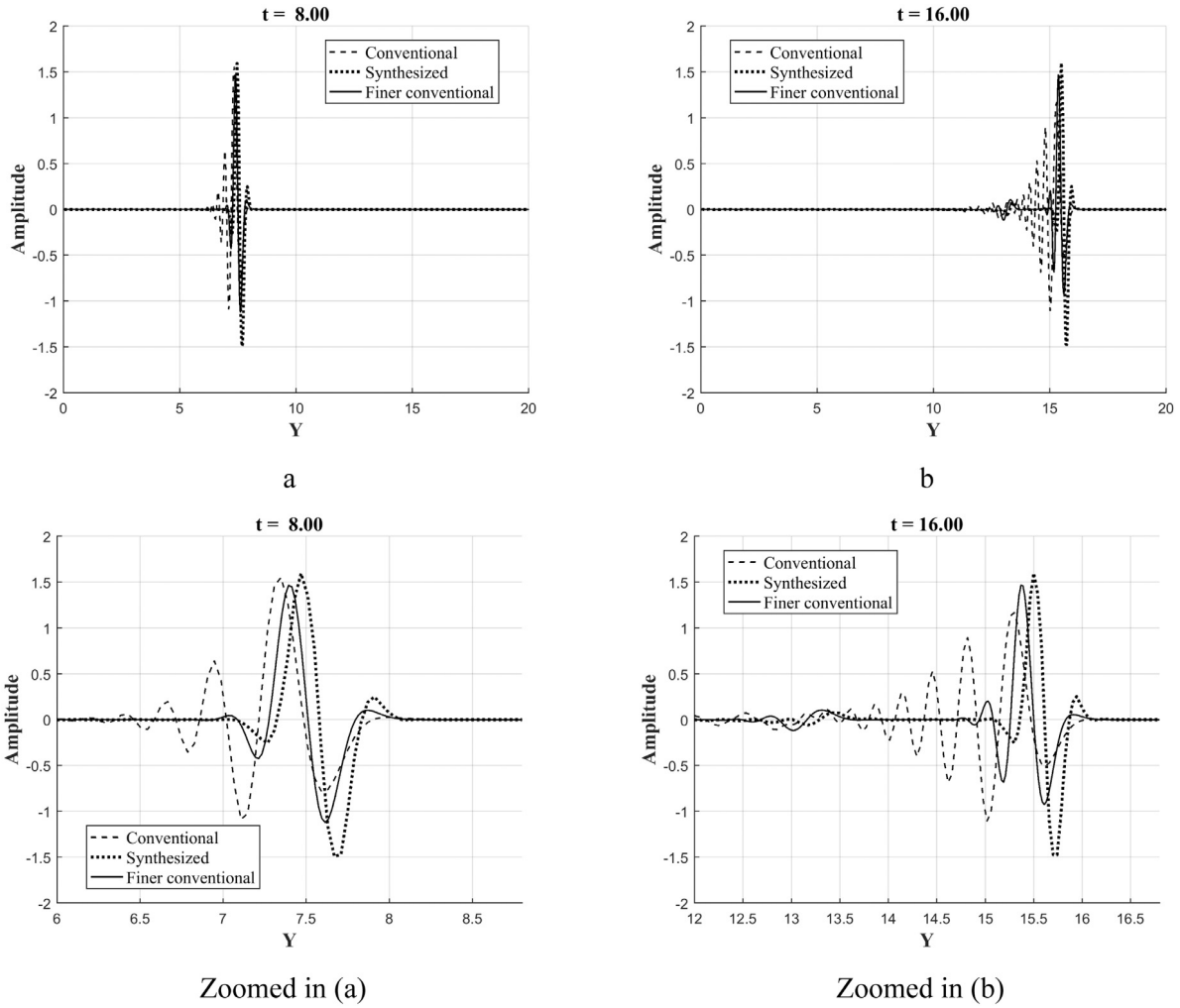

Fig. 5. Values of state variable at central line nodes after the pulse simulation for 8 and 16 pulse periods T. The conventional and synthesized element models consisted of 501 501 nodes, the finer conventional model consisted of 2 003 001 nodes.

wavelength. The model consisted of 48 400 nodes. The finer mesh model with the twice shorter distance between the nodes (∼25 nodes per wavelength) used 367 951 nodes. In order to assign the same boundary conditions for all models, in the synthesized element model the first row of the elements with the nodes in the excitation zone was replaced by the conventional elements.

The obtained distributions of the state variable after 4 pulse periods are provided in Fig. 7 for the model composed of the synthesized elements (Fig. 7b), model of the conventional elements with the same number of nodes as in the model of the synthesized elements (Fig. 7a) and model of the conventional elements with fine mesh as the element side length is twice shorter than in the previous model (Fig. 7c). The resulting state variable values at the central line of the structure along the long side in the pulse area are compared in Fig. 7d. Although the length of the structure is less than 4 pulse periods, it can be clearly seen that the shape of the pulse changed during simulation in the coarse conventional element model. The impulse in the synthesized element model retained its shape and was close to the one obtained using the refined mesh model of conventional elements.

Due to the fact that the number of elements grows as n^3 by refining the mesh, the analysis of the finer mesh model for large structures is limited by computational resources. However, it is still possible to compare the results obtained for the conventional and synthesized models with the same number of nodes. To simulate the pulse propagation for more periods, a higher number of nodes per wavelength is required. For the longer simulation, the side length of the synthesized element was equal to 0.096 resulting the initial distance between the two nodes equal to 0.032 and approximately 16 nodes per wavelength. The rectangular parallelepiped structure of size 12.768 pulse lengths in length and 0.672 pulse lengths in width and height was analyzed in the latter numerical experiments. The pulse propagation was simulated for 12.8 pulse periods T. The B-Scan results are shown in Fig. 8a, b for both conventional and synthesize element models with

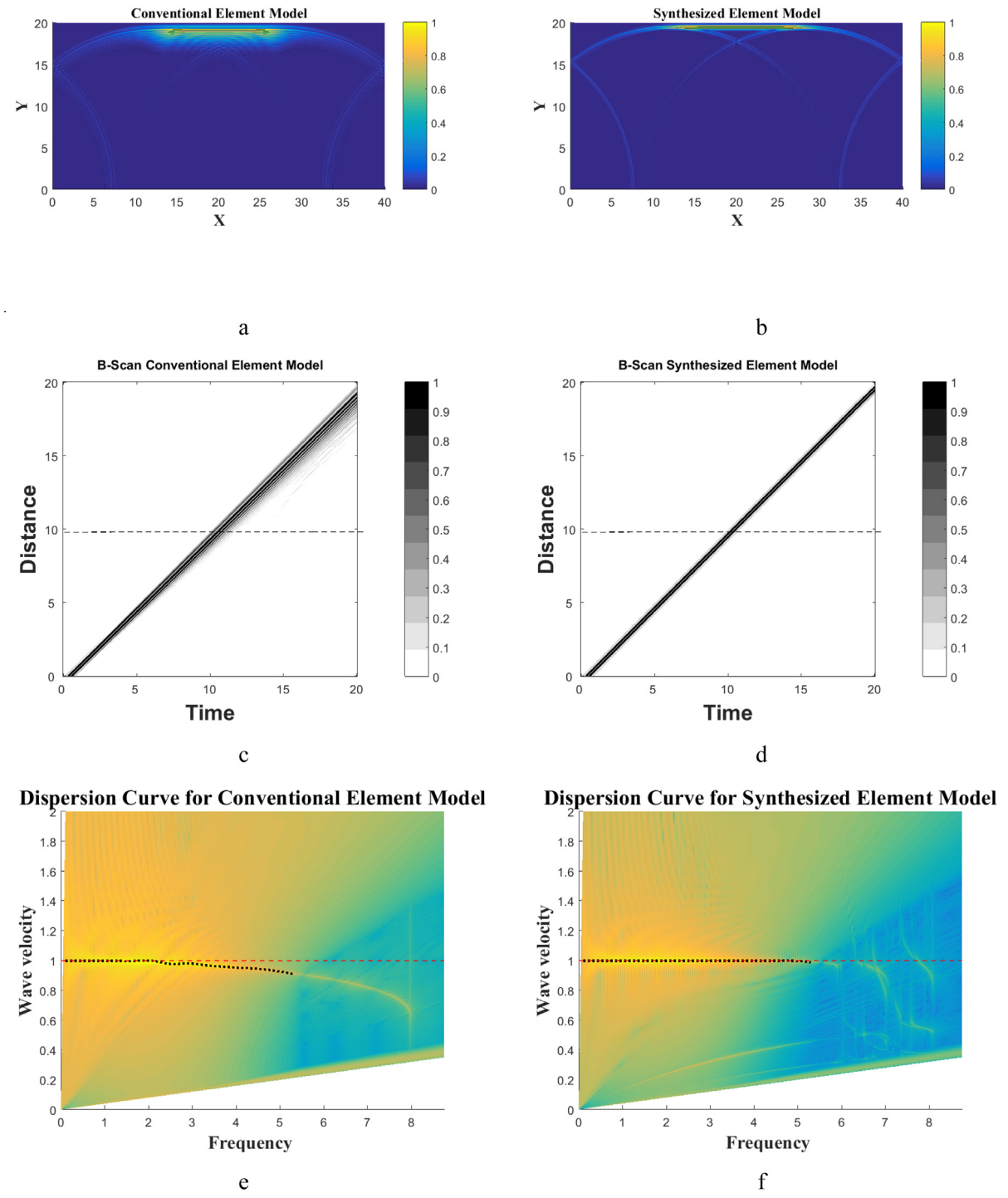

Fig. 6. The distribution of the state variable (a, b), B-scan views (c, d) and dispersion curves (e, f). The figures (a, c, e) represent values for conventional element model and figures (b, d, f) represent synthesized element model. Both models consisted of 501 501 nodes (structure of 1001 × 501 nodes), simulated duration 20 pulse periods T. (For interpretation of the references to color in this figure legend, the reader is referred to the web version of this article.)

the same number of nodes (193 600 nodes). In the ideal case the signal maintains its shape during simulation. It is not possible to compare the results obtained for the finer mesh due to the limitations of the computational resources because

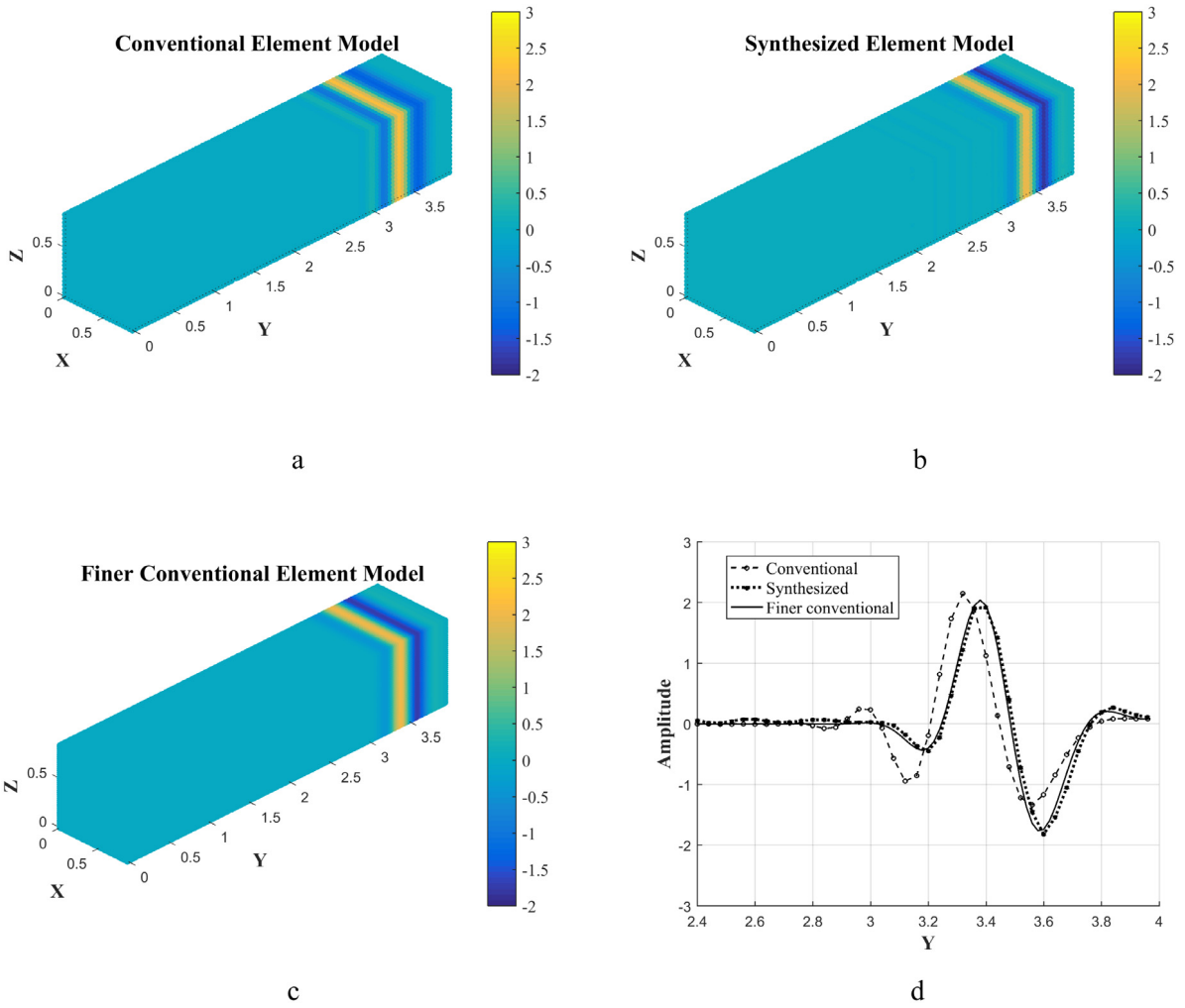

Fig. 7. The comparison of wave propagation in the models composed of conventional elements (48 400 nodes) (a), synthesized elements (48 400 nodes) (b), conventional elements with finer mesh (367 951 nodes) (c) and zoom-in of the amplitude values in the pulse area at the central line of the models (d). Pulse propagation was simulated for 4 pulse periods T.

the mesh with twice shorter distance between the nodes consists of 1 477 351 nodes. It has been shown in Fig. 8 that the pulse disperses in the conventional element model and maintains its shape in the synthesized element model.

The dispersion curves for the conventional and synthesized element models are provided in Fig. 8c, d. The theoretical wave velocity is equal to 1 and is marked by the red dashed line. The black dotted line shows the wave velocities for the maximum amplitude waves of the specific frequency obtained in the simulation. By applying the synthesized elements in the model, the range of the close-to-exact frequencies is expanded approximately by 1.65 times as the curve obtained numerically drops to wave speed of 0.99 at 2.66 for the conventional element model and at 4.38 for the synthesized element model. For the higher frequencies the curve obtained for the synthesized element model has a sharper decrease compared to the curve obtained for the conventional element model, and a wave speed equal to 0.85 for the maximum amplitude waves is observed at approximately 8.11 for both models. The advantage of the synthesized element model is that the speed velocities are close to the theoretical speed velocity in the frequency range of the analyzed impulse.

5. Conclusion

An approach for reduction of the computational resources required for short acoustic wave propagation simulation has been developed and presented in this article. This approach includes construction of a higher-order element by modal synthesis and optimum adjustment of modal frequencies for the individual element. An important novelty of the work is that the mass matrices of the synthesized models are diagonal and well suited for the explicit dynamic analysis. The numerical experiments were performed for the structures in 2D and 3D. The obtained results showed good agreement with

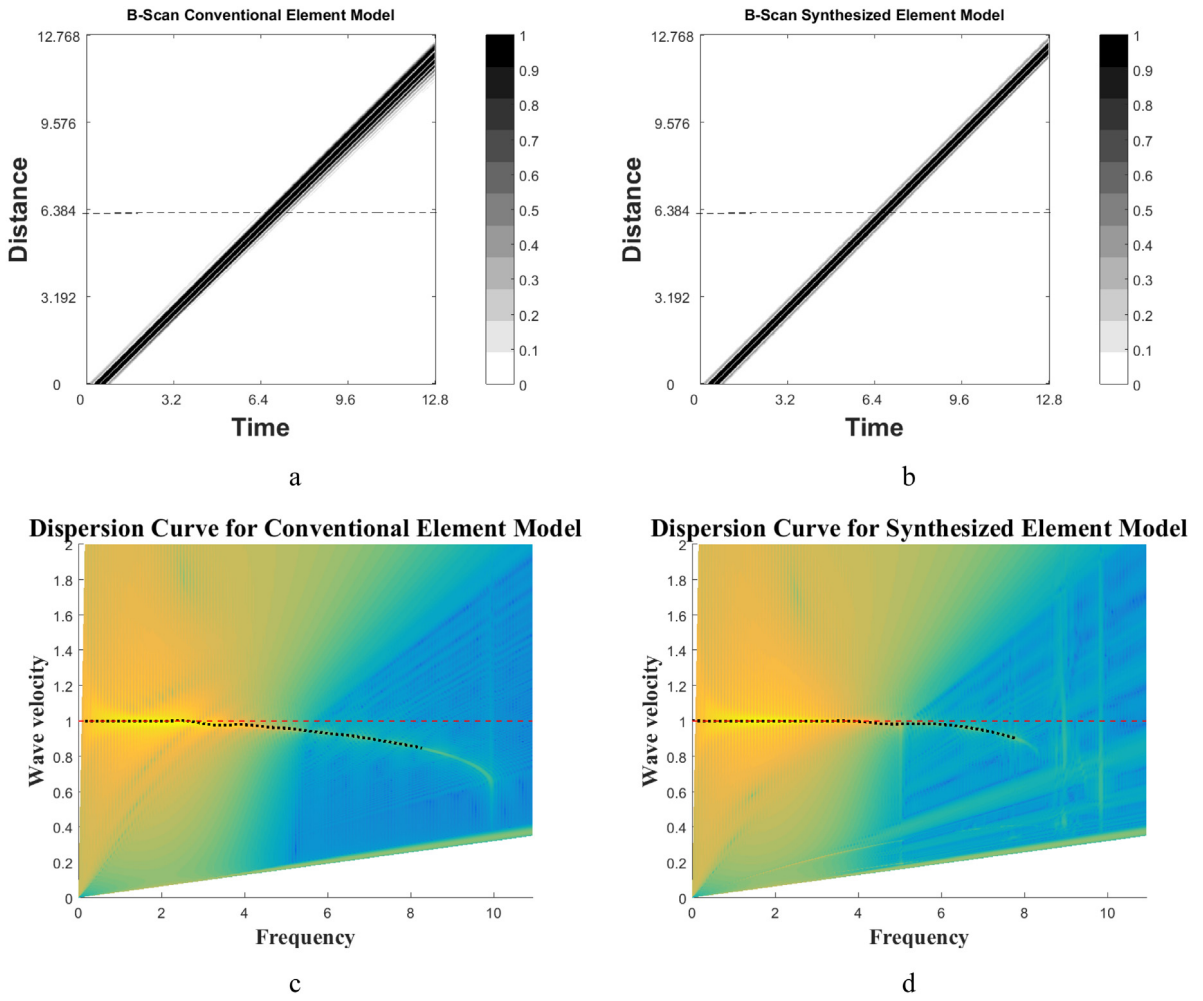

Fig. 8. B-scan results and the dispersion curves for the conventional (a, c) and synthesized (b, d) element models (193 600 nodes), simulated duration was 12.8 pulse periods T. (For interpretation of the references to color in this figure legend, the reader is referred to the web version of this article.)

the ones obtained for the models assembled of conventional elements with twice shorter element side length. Although in some cases due to limited computational resources it was not possible to simulate wave propagation in the finer mesh model and compare the results, the synthesized element model demonstrated good performance based on the B-scan and analysis of the dispersion curves. We should emphasize that the synthesized element performs well if the short wave frequency range corresponds to the frequency range optimized in the synthesis of element.

The number of nodes per wavelength depend on various parameters such as the pulse shape and how long the propagation is modeled. The results showed that the usage of synthesized elements enable to use 13 nodes per wavelength in 2D model to simulate pulse propagation for 15 pulse periods and 16 nodes per wavelength in 3D model to simulate pulse propagation for over 10 pulse periods. The pulse maintains its shape in the synthesized element model and deteriorates in the conventional element model with the same number of nodes. For shorter propagation or signal of simpler shape the smaller number of nodes per wavelength can be used. The reduced number of nodes in the model shortens computational time and required memory resources.

The approach works for regular element shapes such as square in 2D and rectangular parallelepiped in 3D. By using the obtained elements, large internal areas of simulated bodies can be uniformly meshed in elements with modest side lengths. In case of complex geometry domains, the regions in the vicinity of the curved boundaries can be meshed with conventional elements because the synthesized and conventional elements are mutually compatible.

Declaration of competing interest

The authors declare that they have no known competing financial interests or personal relationships that could have appeared to influence the work reported in this paper.

Appendix

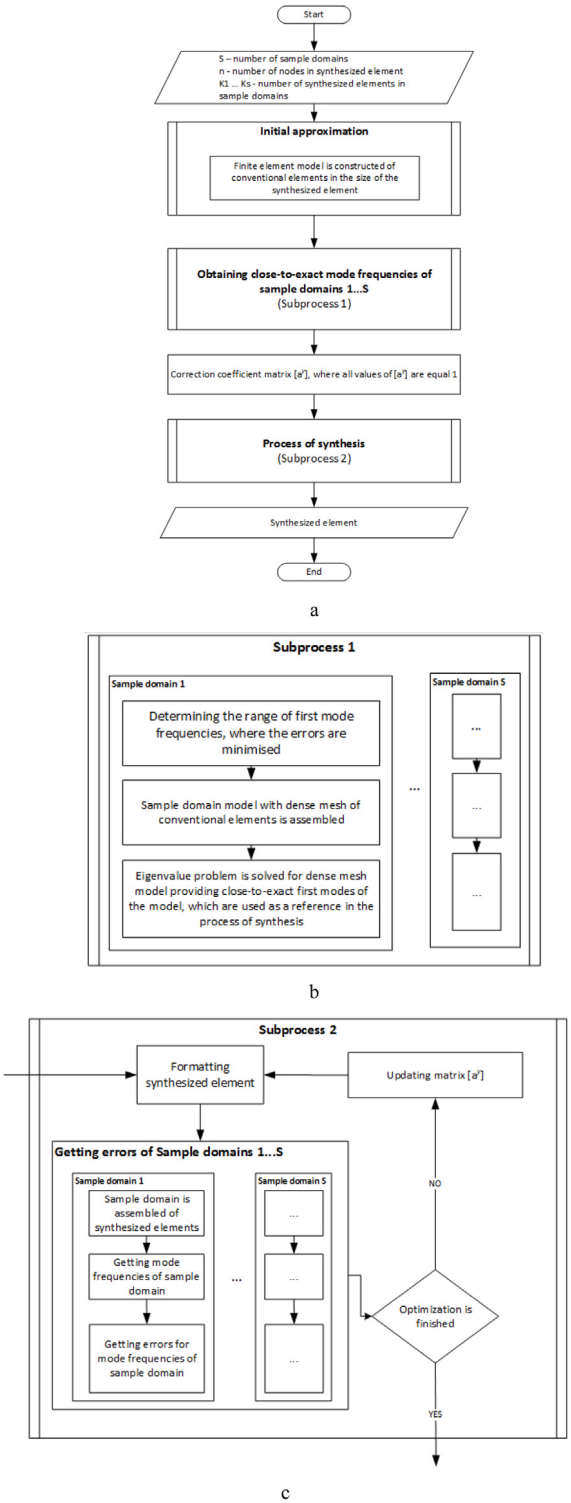

Fig. A.1. Flowchart of the FE synthesis procedure.

References

[1] A. El Kacimi, O. Laghrouche, M.S. Mohamed, J. Trevelyan, Bernstein–Bézier based finite elements for efficient solution of short wave problems, Comput. Methods Appl. Mech. Engrg. 343 (2019) 166–185, http://dx.doi.org/10.1016/j.cma.2018.07.040.

[2] O. Laghrouche, P. Bettess, R.J. Astley, Modelling of short wave diffraction problems using approximating systems of plane waves, Internat. J. Numer. Methods Engrg. 54 (2002) 1501–1533, http://dx.doi.org/10.1002/nme.478.

[3] O.C. Zienkiewicz, R.L. Taylor, The Finite Element Method, Elsevier, 2005.

[4] J. Gu, Y. Jing, Modeling of wave propagation for medical ultrasound: A review, IEEE Trans. Ultrason. Ferroelectr. Freq. Control 62 (2015) 1979–1993, http://dx.doi.org/10.1109/TUFFC.2015.007034.

[5] D. Komatitsch, G. Erlebacher, D. Göddeke, D. Michéa, High-order finite-element seismic wave propagation modeling with MPI on a large GPU cluster, J. Comput. Phys. 229 (2010) 7692–7714, http://dx.doi.org/10.1016/j.jcp.2010.06.024.

[6] S. Liu, X. Li, W. Wang, Y. Liu, A mixed-grid finite element method with PML absorbing boundary conditions for seismic wave modelling, J. Geophys. Eng. 11 (2014) http://dx.doi.org/10.1088/1742-2132/11/5/055009.

[7] R.S. Schechter, H.H. Chaskelis, R.B. Mignogna, P.P. Delsanto, Real-time parallel computation and visualization of ultrasonic pulses in solids, Science (80-.). 265 (1994) 1188–1192, http://dx.doi.org/10.1126/science.265.5176.1188.

[8] R. Barauskas, R. Barauskiene, Highly convergent dynamic models obtained by modal synthesis with application to short wave pulse propagation, Internat. J. Numer. Methods Engrg. 61 (2004) 2536–2554, http://dx.doi.org/10.1002/nme.1169.

[9] C.T. Nguyen, J.L. Tassoulas, Application of reciprocal absorbing boundary condition to transient analysis of acoustic wave propagation, Comput. Methods Appl. Mech. Engrg. 329 (2018) 55–74, http://dx.doi.org/10.1016/j.cma.2017.09.023.

[10] M. Ganesh, C. Morgenstern, High-order FEM domain decomposition models for high-frequency wave propagation in heterogeneous media, Comput. Math. Appl. 75 (2018) 1961–1972, http://dx.doi.org/10.1016/j.camwa.2017.10.041.

[11] I. Bartoli, A. Marzani, F. Lanza di Scalea, E. Viola, Modeling wave propagation in damped waveguides of arbitrary cross-section, J. Sound Vib. 295 (2006) 685–707, http://dx.doi.org/10.1016/j.jsv.2006.01.021.

[12] J. Wu, Z. Tang, F. Lü, K. Yang, Ultrasonic guided wave focusing in waveguides with constant irregular cross-sections, Ultrasonics 89 (2018) 1–12, http://dx.doi.org/10.1016/j.ultras.2018.04.003.

[13] F. Casadei, J.J. Rimoli, M. Ruzzene, Multiscale finite element analysis of wave propagation in periodic solids, Finite Elem. Anal. Des. 108 (2016) 81–95, http://dx.doi.org/10.1016/j.finel.2015.10.002.

[14] B. Yue, M.N. Guddati, Dispersion-reducing finite elements for transient acoustics, J. Acoust. Soc. Am. 118 (2005) 2132–2141, http://dx.doi.org/10.1121/1.2011149.

[15] Y. Mirbagheri, H. Nahvi, J. Parvizian, A. Düster, Reducing spurious oscillations in discontinuous wave propagation simulation using high-order finite elements, Comput. Math. Appl. 70 (2015) 1640–1658, http://dx.doi.org/10.1016/j.camwa.2015.06.022.

[16] Z. Zuo, S. Li, C. Zhai, L. Xie, Optimal lumped mass matrices by minimization of modal errors for beam elements, J. Vib. Acoust. 136 (2014) 21015, http://dx.doi.org/10.1115/1.4026247.

[17] Z.C. He, E. Li, G.R. Liu, G.Y. Li, A.G. Cheng, A mass-redistributed finite element method (MR-FEM) for acoustic problems using triangular mesh, J. Comput. Phys. 323 (2016) 149–170, http://dx.doi.org/10.1016/j.jcp.2016.07.025.

[18] R. Khajavi, General templates for n-noded bar elements based on reduced representations and numerical dispersion reduction by optimized finite elements, Appl. Math. Comput. 233 (2014) 445–462, http://dx.doi.org/10.1016/j.amc.2014.02.022.

[19] E. Li, Z.C. He, Z. Zhang, G.R. Liu, Q. Li, Stability analysis of generalized mass formulation in dynamic heat transfer, Numer. Heat Transfer B 69 (2016) 287–311, http://dx.doi.org/10.1080/10407790.2015.1104215.

[20] G. Noh, K.J. Bathe, An explicit time integration scheme for the analysis of wave propagations, Comput. Struct. 129 (2013) 178–193, http://dx.doi.org/10.1016/j.compstruc.2013.06.007.

[21] A.V. Idesman, D. Pham, Finite element modeling of linear elastodynamics problems with explicit time-integration methods and linear elements with the reduced dispersion error, Comput. Methods Appl. Mech. Engrg. 271 (2014) 86–108, http://dx.doi.org/10.1016/j.cma.2013.12.002.

[22] W. Liao, P. Yong, H. Dastour, J. Huang, Efficient and accurate numerical simulation of acoustic wave propagation in a 2D heterogeneous media, Appl. Math. Comput. 321 (2018) 1339–1351, http://dx.doi.org/10.1016/j.amc.2017.10.052.

[23] A. Kriščiūnas, R. Barauskas, Highly convergent finite elements with diagonal mass matrix for short wave pulse propagation simulation, Inf. Technol. Control 45 (2016) 308–320, http://dx.doi.org/10.5755/j01.itc.45.3.13557.

[24] A. Krisciunas, Development of Highly Convergent Numerical Algorithms for Short Elastic Wave Simulation Summary of Doctoral Dissertation, Kaunas University of Technology, 2017.

[25] S. Liu, D. Yang, C. Lang, W. Wang, Z. Pan, Modified symplectic schemes with nearly-analytic discrete operators for acoustic wave simulations, Comput. Phys. Comm. 213 (2017) 52–63, http://dx.doi.org/10.1016/j.cpc.2016.12.002.

[26] O.C. Zienkiewicz, R.L. Taylor, 7. steady-state field problems - heat conduction, electric and magnetic potential, fluid flow, etc, in: Finite Elem. Method Vol. 1, Basis, Elsevier, New York, 2000.

[27] D. Maity, S. Kumar Bhattacharyyab, A parametric study on fluid–structure interaction problems, J. Sound Vib. 263 (2003) 917–935, http://dx.doi.org/10.1016/S0022-460X(02)01079-9.

[28] H.C. Chen, R.L. Taylor, Vibration analysis of fluid–solid systems using a finite element displacement formulation, Internat. J. Numer. Methods Engrg. 29 (1990) 683–698, http://dx.doi.org/10.1002/nme.1620290402.

[29] B.R. Mace, E. Manconi, Modelling wave propagation in two-dimensional structures using finite element analysis, J. Sound Vib. 318 (2008) 884–902, http://dx.doi.org/10.1016/j.jsv.2008.04.039.

[30] R. Kažys, L. Mažeika, R. Barauskas, E. Jasiūnienė, V. Daniulaitis, Evaluation of diffraction errors in precise pulse-echo measurements of ultrasound velocity in chambers with waveguide, Ultrasonics 40 (2002) 853–858, http://dx.doi.org/10.1016/S0041-624X(02)00226-3.

[31] Y. Luo, J. Xia, R.D. Miller, Y. Xu, J. Liu, Q. Liu, Rayleigh-wave dispersive energy imaging using a high-resolution linear radon transform, Pure Appl. Geophys. 165 (2008) 903–922, http://dx.doi.org/10.1007/s00024-008-0338-4.